Role of ^{18}F-FDG PET/CT in Erdheim–Chester Disease in the Era of Multimodality Imaging

Bhargavi Jois[1]   Rupa Ananthasivan[2]   Parameswaran R. V. Sudarshan Rawat[2]   Susmita Rakshit[3]

[1] Department of Nuclear Medicine, Manipal Hospitals, Bengaluru, Karnataka, India
[2] Department of Radiology, Manipal Hospitals, Bengaluru, Karnataka, India
[3] Department of Pathology, Manipal Hospitals, Bengaluru, Karnataka, India

Address for correspondence Bhargavi Jois, Department of Nuclear Medicine, Manipal Hospitals, 98, HAL Airport Road, Kodihalli, Bengaluru 560 017, Karnataka, India
(e-mail: bhargavijois@gmail.com).

Abstract

Erdheim–Chester disease is a rare disease with systemic non-Langerhans cell histiocytosis, the diagnosis of which with conventional imaging modalities is challenging. We describe a case of a 73-year-old woman who was referred with a progressive history of bilateral proptosis. The magnetic resonance imaging (MRI) orbit demonstrated bilateral orbital masses with optic nerve encasement. A subsequent 18F-FDG PET/CT scan showed multi-organ disease with involvement of the orbits, pericardium, aorta, pararenal fascia, and appendicular bones. Metabolically active, easily accessible areas were selected for CT-guided biopsy. The biopsy showed sheets of foamy histiocytes with the expression of CD 68 and CD 163 consistent with a diagnosis of Erdheim–Chester disease. The FDG PET/CT played a pivotal role in establishing the diagnosis with the assessment of disease extent and further guided in the targeted biopsy.

Keywords
► Erdheim–Chester disease
► FDG PET/CT
► multimodality imaging

Introduction

Erdheim–Chester disease (ECD) is a systemic non-Langerhans cell histiocytosis characterized by multi-organ accumulation of foamy histiocytes. Owing to its rarity[1] and varied presentation, ECD presents diagnostic challenges to the clinician and imageologist.

Radiography, CT, and MRI assist in the focused evaluation. ^{18}F-FDG PET/CT plays a vital role in the diagnosis, detection of disease extent and severity, assessment for an appropriate biopsy, and treatment response.[2–5]

We present a case of ECD with multi-system involvement with a discussion of the imaging findings highlighting the importance of FDG-PET/CT.

Case History

A 73-year-old woman presented with a history of gradually progressive right proptosis followed by the left with no diminution of vision.

MRI orbit demonstrated bilateral intra and extraconal soft tissue masses causing exophthalmos with optic nerve encasement (►**Figs. 1** and **2A–C**). Magnetic resonance imaging (MRI) of the brain showed no abnormality. Biopsy of the orbital mass was suggestive of necrobiotic xanthogranuloma. Immunohistochemistry (IHC), however, was not available. She was suspected to have ECD due to retro-orbital involvement. A ^{99m}Tc-methylene diphosphonate bone scan was performed that revealed a characteristic increase in the
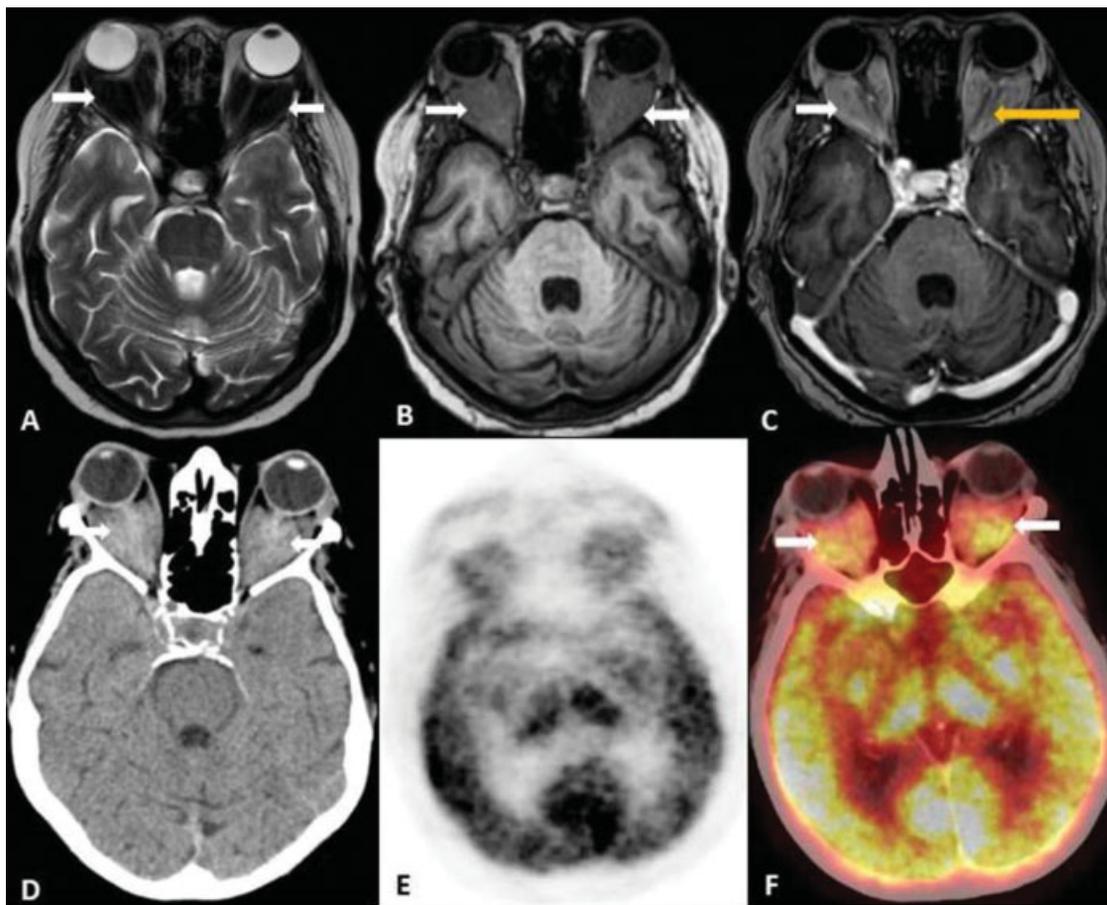
Fig. 1 T2-weighted axial MRI (**A**) showing intraconal hypointense masses encasing the extraocular muscles (white arrow). T1-weighted axial image (**B**) demonstrating the isointense nature of orbital masses (white arrow). Post-contrast T1-weighted axial image (**C**) showing intense enhancement of the intraconal masses (white arrow) with encasement of the optic nerves (yellow arrow). Non-contrast CT (**D**) demonstrating hypodense masses involving the intra- and extraconal compartments with increased FDG uptake seen in corresponding regions on PET (**E**) and fusion PET/CT images (**F**). FDG, fluorodeoxyglucose; PET/CT, positron emission tomography-computed tomography; MRI, magnetic resonance imaging.
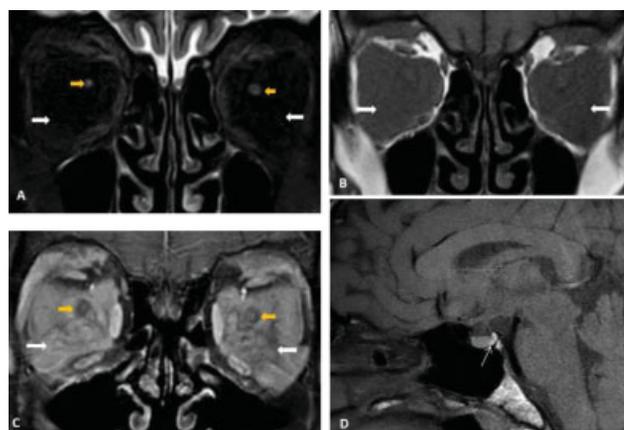

Fig. 2 T2-weighted coronal MRI (**A**) showing hypointense intraconal masses (white arrows) encasing the optic nerve (yellow arrows). T1-weighted coronal MRI (**B**) demonstrating orbital masses, which are isointense to the muscle (white arrow). Post-contrast T1-weighted coronal MRI (**C**) showing avid enhancement of the intraconal masses (white arrow) with encasement of the optic nerves (yellow arrow). TI-weighted sagittal image (**D**) demonstrating normal hyperintense signal of the neurohypophysis (thin white arrow). MRI, magnetic resonance imaging.

osteoblastic activity in the diametaphyses of the long bones of the lower limb centered around the knees (►**Fig. 3A** and **3B**) along with mandibular uptake.

She received interferon-α 2B and intravenous methyl-prednisolone. However, her symptoms worsened with sudden diminution of vision and development of bone pains and hence she was referred to our hospital for further evaluation.

An FDG-PET/CT scan was requested to assess for the extraosseous disease.

The PET/CT showed metabolically active enhancing retrobulbar soft tissue masses corresponding to the MR findings with optic nerve compression and SUV$_{max}$ of 13.2 (►**Fig. 1E** and **1F**).

Widened metadiaphyses were observed in the appendicular bones with cortical thickening and increased metabolic activity—SUV$_{max}$ of 8.2. FDG avidity was also seen in the mandible (►**Fig. 3C–3E**).

FDG avid soft tissue thickening was seen around the aorta and its branches, pericardium, and bilateral posterior pararenal fascia, with SUV$_{max}$ of 6.0 (►**Figs. 4,5,6**).

The PET/CT findings supported the diagnoses of ECD and confirmed multi-organ involvement. Metabolically active, easily accessible areas in the right pararenal region were selected for CT-guided biopsy. A second biopsy was
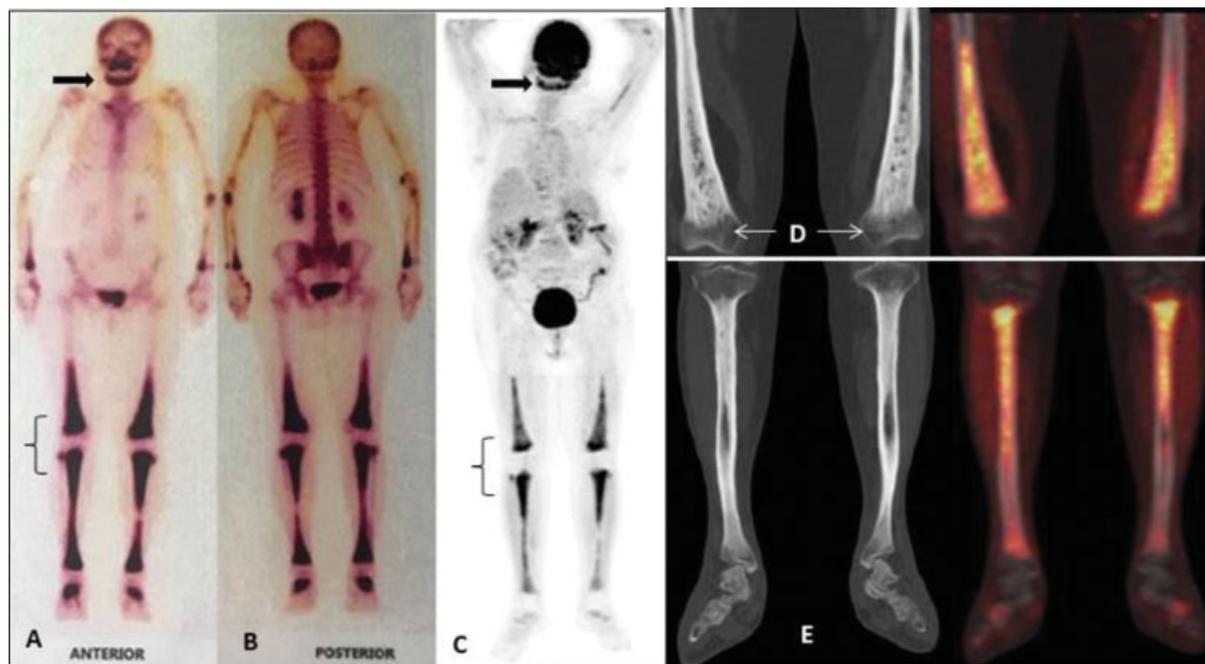
Fig. 3 Anterior (**A**) and posterior (**B**) images of bone scan showing increased osteoblastic activity in the mandible (black arrow), radius, ulna, shafts of tibia and femora. The MIP image of PET scan (**C**) showing FDG avidity in the mandible (black arrow) and lower limb long bones centered on the knees—hot-knee pattern (bracket). Coronal CT; PET/CT Images (**D** and **E**) of the lower limbs (bone window) demonstrating metabolically active bilateral symmetrical osteosclerosis of the diametaphyses of long bones with characteristic sparing of the epiphysis (white arrow). MIP, maximum intensity projection; MRI, magnetic resonance imaging; PET/CT, positron emission tomography-computed tomography.
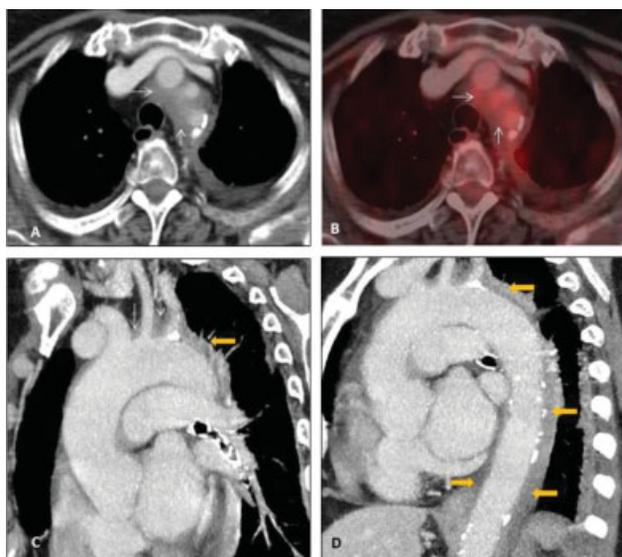

Fig. 4 CECT of the upper chest (**A**) and PET/CT (**B**) showing circumferential hypodense, plaque-like hypermetabolic soft tissue encasing the arch of the aorta and its branches (white arrows). Oblique–sagittal reformatted image of the thoracic aorta (**C** and **D**) shows hypodense plaque-like soft tissue around the branches of the aortic arch (white arrows) and encasing the descending thoracic aorta —coated aorta sign (yellow arrows). CECT, contrast-enhanced computed tomography. PET/CT, positron emission tomography-computed tomography.

warranted to assess IHC and mutational status, particularly with the worsening of symptoms as targeted therapy was being considered. The biopsy showed sheets of foamy histiocytes (►**Fig. 6D**), consistent with ECD. Immunohis-

tochemistry showed the expression of CD 68 and CD 163 and was negative for S-100, CD1a, and Langerin. BRAF mutation was negative.

Owing to a negative BRAF mutation status, targeted therapy was not feasible. She was treated with high-dose dexamethasone, cyclophosphamide, and vincristine to which there was an initial response but the patient subsequently succumbed to the cardiac complications of ECD.

Discussion

ECD is a subset of non-Langerhans cell histiocytosis, first described by William Chester and Jakob Erdheim in 1930.[6]

The diagnosis is often delayed due to the rarity of the disease, multi-organ involvement, and varied presentation.[7] Imaging including ^{18}F-FDG PET/CT plays an important role in the diagnosis, assessing the extent and evaluating the treatment response.[2–5,7]

Up to 96% of patients show skeletal involvement,[8,9] like our patient. The ^{99m}Tc-methylene diphosphonate bone scan and the FDG-PET showed intense, bilaterally symmetric uptake at the end of long bones centered around the knees with sparing of the epiphysis—"hot-knee pattern" (►**Fig. 3**), which is characteristic of ECD.[7,10] The CT demonstrated corresponding symmetrical osteosclerosis of the diametaphyses of the long bones with loss of corticomedullary differentiation, no periostitis, and epiphyseal sparing[11] (►**Fig. 3D** and **3E**). FDG-PET and bone scan uptake can precede radiographic abnormalities.[7,12]

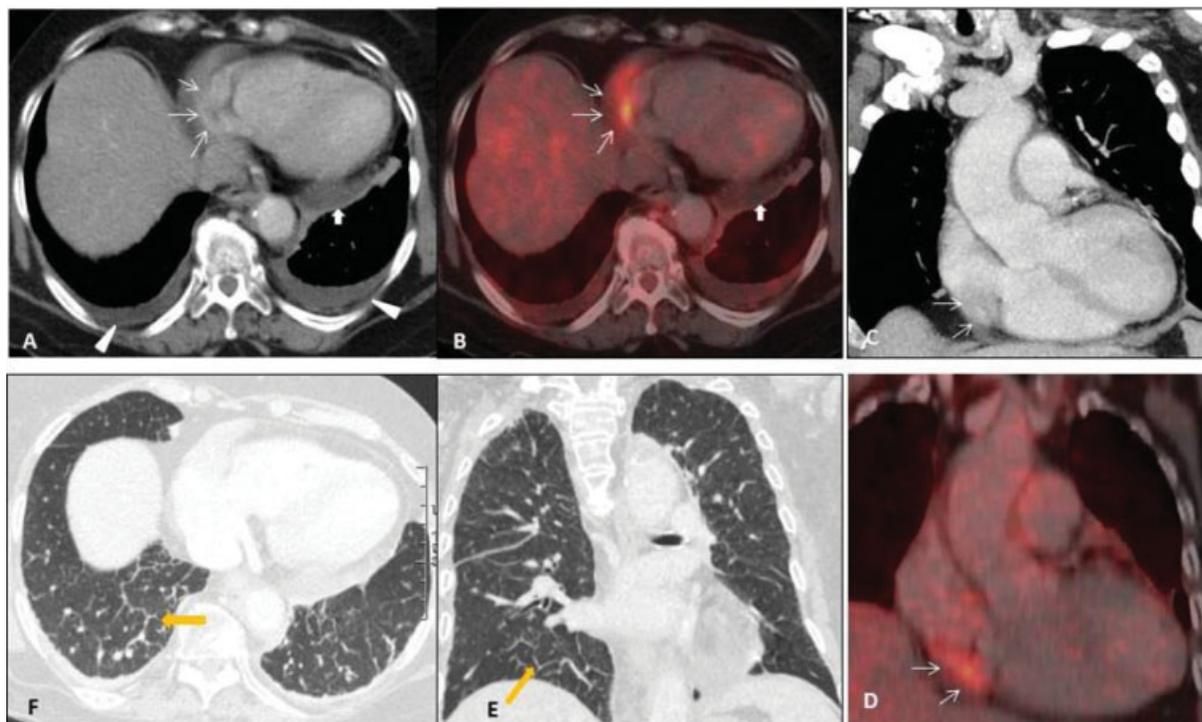Orbital involvement is present in up to 38%.[8,9,13] Exophthalmos was the initial presentation of our patient. The

Fig. 5 (A–F, clockwise) CECT (**A**) and PET/CT (**B**) showing smooth plaque-like hypermetabolic thickening mainly involving the right side of the heart (thin white arrows), pericardial thickening with effusion (bold white arrow), and bilateral pleural effusion (arrowheads). Coronal reformatted CECT (**C**) and PET/CT (**D**) images showing plaque-like hypermetabolic soft tissue in relation to the right atrium (white arrows). Axial (**E**) and coronal images (**F**) of the CT chest (lung window) demonstrating septal thickening in the lung bases (bold yellow arrows). CECT, contrast-enhanced computed tomography; PET/CT, positron emission tomography-computed tomography.
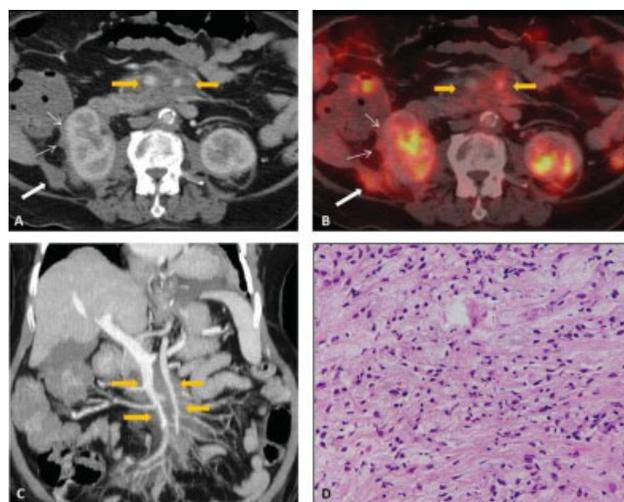

Fig. 6 Hairy kidney sign–CECT (**A**) demonstrating perirenal fat infiltration with a characteristic spiculated appearance (thin white arrow) and enhancing pararenal soft tissue masses (bold white arrow). PET/CT (**B**) demonstrating the hypermetabolic nature of perirenal and pararenal soft tissue thickening (thin white arrows and bold white arrows, respectively). Coronal reformatted MIP image of CECT abdomen (**C**) showing circumferential soft tissue encircling the mesenteric vessels; which is also seen in images **A** and **B** (yellow arrows). Histology (**D**) showing sheets of foamy histiocytes. CECT, contrast-enhanced computed tomography; MIP, maximum intensity projection.

initial biopsy suggested necrobiotic xanthogranuloma, which commonly presents as anterior orbital or ocular

adnexal lesions.[14] The retro-orbital involvement led to the suspicion of ECD. The MRI revealed classic T1 and T2 hypo-intense multi-compartmental retro-orbital masses encasing the optic nerve (►**Figs. 1** and **2**). PET/CT showed corresponding increased metabolic activity (►**Fig. 1**) with SUV$_{max}$ of 13 similar to other studies.[7]

Imaging plays a vital role in surgical planning, particularly in the orbit. The exquisite soft-tissue contrast of MRI helps planning for surgical decompression, particularly if the optic nerve is at risk. Imaging including PET/CT, which identifies active tissue, helps the ophthalmologist choose the best site for biopsy.

CNS involvement is seen in more than half of cases and is a leading cause of death.[8] The absence of a normal T1 hyperintense signal of the neurohypophysis, dural, and meningeal involvement and symmetrical T2-hyperintensities of the dentate nucleus have been described.[8,9]

The CNS involvement with increased FDG uptake has been linked to the *BRAF* gene mutation.[7] Our patient did not show CNS involvement and was *BRAF* gene-negative.

Cardiovascular involvement is seen in nearly three-fourths of cases and presents either as circumferential infiltration of the adventitia of the blood vessels, commonly involving the aortic arch or as pericardial infiltration or rarely as right-sided myocardial involvement.[4,15–17]

PET/CT in our patient revealed hypermetabolic hypodense, plaque-like soft tissue circumferentially encasing the aorta and its branches (►**Fig. 4**)—described as the "coated aorta sign."[7,8] It also showed smooth plaque-like thickening

involving the right side of the heart, together with pericardial thickening and effusion (►**Fig. 5A–D**).

Cardiovascular involvement indicates a poor prognosis and leads to death in ~60% of cases due to tamponade, arrhythmias, or infarction.[8,18] Our patient expired due to cardiovascular complications of ECD.

The lung and pleura are affected in ~40 to 50% of cases[8] as smooth inter- and intralobular septal thickening[19] as was demonstrated in our patient (►**Fig. 5E** and **5F**).

The retroperitoneum including the kidneys is involved in ~68% of cases.[4,8] Our patient had FDG avid soft tissue masses in bilateral perirenal and posterior pararenal spaces (►**Fig. 6A** and **6B**). The hairy kidney sign refers to perirenal fat infiltration seen in ECD with a characteristic spiculated appearance,[4,7,8] which was seen quite elegantly on the PET/CT (►**Fig. 6A** and **6B**) with corresponding FDG uptake.

^{18}F-FDG PET/CT assists in differentiating ECD from Langerhans histiocytosis (LCH), Rosai–Dorfman Disease (RDD), IgG4-related disease, idiopathic retroperitoneal fibrosis, and sarcoidosis.[8]

Generally, LCH manifests earlier than ECD. The bony involvement in LCH is characteristically osteolytic and involves the skull, spine, or long bones asymmetrically unlike the symmetrical osteosclerosis seen in ECD, which involves the ends of the long bones. Cardiac involvement is rare in LCH.[20]

RDD may show right heart involvement similar to ECD but bony involvement is characteristically osteolytic.[20] Lymphadenopathy especially in more than one region with moderate to high ^{18}F-FDG avidity is seen in RDD.

Specific FDG-PET/CT patterns have been described in IgG4-RD—diffusely increased ^{18}F-FDG uptake in the pancreas and salivary glands, patchy lesions in the retroperitoneal region and vascular wall, and multi-organ involvement.[21] Retroperitoneal fibrosis (RPF), retro-orbital involvement, and pachymeningitis are common features between ECD and IgG4-RD. RPF associated with ECD generally affects the perirenal areas with resultant proximal ureteric obstruction. RPF associated with IgG4-related disease usually results in distal ureteric obstruction with medial deviation.[22]

Idiopathic RPF shows lower FDG uptake as compared with secondary RPF as seen in ECD.[23]

Sarcoidosis shows similarity with ECD as far as the CNS and pulmonary findings are considered but the characteristic bony or vascular changes have not been described.[8] Sarcoidosis, in turn, is characterized by metabolically active lymphadenopathy.

Although the bone scan is a sensitive tool to assess skeletal involvement in ECD,[10] evaluation of the bone marrow is not possible. PET/CT not only evaluates skeletal involvement but also occult visceral, vascular, and bone marrow involvement. FDG-PET hence helps choose the best site for biopsy.

The Annual ECD Medical Symposium Consensus 2020 guidelines recommend multicore biopsies from the most FDG-avid sites that are accessible and safe as histiocytic infiltration may be heterogeneous.[24] The right posterior pararenal FDG avid soft tissue masses, which were easily and safely accessible, were chosen for repeat biopsy in our patient.

These guidelines also recommend *BRAF* mutational status to initiate BRAF V 600E inhibitor therapy.[24] As the *BRAF* mutational status in our patient was negative, targeted therapy was not feasible.

If targeted therapies are unavailable or not indicated, treatment depends on the active disease burden, wherein PET-CT plays an important role.[24]

Tissue fibrosis can occur in ECD and hence an evaluation of metabolic rather than anatomic treatment response is essential with a follow-up PET-CT 3 to 6 months after the initiation of therapy.[24]

Hence, ^{18}F-FDG-PET/CT plays an important role in patients with ECD not only in the diagnoses but also in the evaluation of disease extent as a guiding tool for targeted biopsies and assessment for treatment response.

References

1 Stempel JM, Bustamante Alvarez JG, Carpio AM, Mittal V, Dourado C. Erdheim-Chester disease, moving away from the orphan diseases: a case report. Respir Med Case Rep 2016;20:55–58

2 Girszyn N, Arnaud L, Villain D, Kahn JE, Piette AM, Bletry O. Usefulness of combined positron emission tomography and computed tomography imaging in Erdheim-Chester disease [article in French]. Rev Med Interne 2007;28(11):770–774

3 Arnaud L, Malek Z, Archambaud F, et al. 18F-fluorodeoxyglucose-positron emission tomography scanning is more useful in followup than in the initial assessment of patients with Erdheim-Chester disease. Arthritis Rheum 2009;60(10):3128–3138

4 Antunes C, Graça B, Donato P. Thoracic, abdominal and musculoskeletal involvement in Erdheim-Chester disease: CT, MR and PET imaging findings. Insights Imaging 2014;5(04):473–482

5 Sioka C, Estrada-Veras J, Maric I, Gahl WA, Chen CC. FDG PET images in a patient with Erdheim-Chester disease. Clin Nucl Med 2014;39(02):170–177

6 Chester W. Über lipoid granulomatose. Virchows Arch Pathol Anat 1930;279:561–602

7 Young JR, Johnson GB, Murphy RC, Go RS, Broski SM. 18F-FDG PET/CT in Erdheim-Chester disease: imaging findings and potential BRAF mutation biomarker. J Nucl Med 2018;59(05):774–779

8 Kumar P, Singh A, Gamanagatti S, Kumar S, Chandrashekhara SH. Imaging findings in Erdheim-Chester disease: what every radiologist needs to know. Pol J Radiol 2018;83:e54–e62

9 Lodhi U, Sarmast U, Khan S, Yaddanapudi K. Multisystem radiologic manifestations of Erdheim-Chester disease. Case Rep Radiol 2016;2016:2670495

10 García-Gómez FJ, Acevedo-Báñez I, Martínez-Castillo R, et al. The role of 18FDG, 18FDOPA PET/CT and 99mTc bone scintigraphy imaging in Erdheim-Chester disease. Eur J Radiol 2015;84(08):1586–1592

11 Dion E, Graef C, Miquel A, et al. Bone involvement in Erdheim-Chester disease: imaging findings including periostitis and partial epiphyseal involvement. Radiology 2006;238(02):632–639

12 White TV, Silvester NC, Otero HJ. Non-sclerotic bone involvement in Erdheim-Chester: PET/CT and MRI findings in a 15-year-old boy. Pediatr Radiol 2016;46(09):1345–1349

13 De Abreu MR, Chung CB, Biswal S, Haghighi P, Hesselink J, Resnick D. Erdheim-Chester disease: MR imaging, anatomic, and

histopathologic correlation of orbital involvement. Am J Neuro-radiol 2004;25(04):627–630

14 Sivak-Callcott JA, Rootman J, Rasmussen SL, et al. Adult xanthog-ranulomatous disease of the orbit and ocular adnexa: new immunohistochemical findings and clinical review. Br J Ophthal-mol 2006;90(05):602–608

15 Munoz J, Janku F, Cohen PR, Kurzrock R. Erdheim-Chester disease: characteristics and management. Mayo Clin Proc 2014;89(07): 985–996

16 Dion E, Graef C, Haroche J, et al. Imaging of thoracoabdominal involvement in Erdheim-Chester disease. AJR Am J Roentgenol 2004;183(05):1253–1260

17 Haroche J, Cluzel P, Toledano D, et al. Images in cardiovascular medicine. Cardiac involvement in Erdheim-Chester disease: magnet-ic resonance and computed tomographic scan imaging in a mono-centric series of 37 patients. Circulation 2009;119(25):e597–e598

18 Alharthi MS, Calleja A, Panse P, et al. Multimodality imaging showing complete cardiovascular involvement by Erdheim-Chester disease. Eur J Echocardiogr 2010;11(07):E25

19 Rush WL, Andriko JA, Galateau-Salle F, et al. Pulmonary pathology of Erdheim-Chester disease. Mod Pathol 2000;13(07):747–754

20 Goyal G, Young JR, Koster MJ, et al; Mayo Clinic Histiocytosis Working Group. The Mayo Clinic Histiocytosis Working Group consensus statement for the diagnosis and evaluation of adult patients with histiocytic neoplasms: Erdheim-Chester disease, langerhans cell histiocytosis, and Rosai-Dorfman disease. Mayo Clin Proc 2019;94(10):2054–2071

21 Zhang J, Chen H, Ma Y, et al. Characterizing IgG4-related disease with ^{18}F-FDG PET/CT: a prospective cohort study. Eur J Nucl Med Mol Imaging 2014;41(08):1624–1634

22 Haroche J, Cohen-Aubart F, Rollins BJ, et al. Histiocytoses: emerging neoplasia behind inflammation. Lancet Oncol 2017;18(02):e113–e125

23 Wang Y, Guan Z, Gao D, et al. The value of ^{18}F-FDG PET/CT in the distinction between retroperitoneal fibrosis and its malignant mimics. Semin Arthritis Rheum 2018;47(04):593–600

24 Goyal G, Heaney ML, Collin M, et al. Erdheim-Chester disease: consensus recommendations for evaluation, diagnosis, and treat-ment in the molecular era. Blood 2020;135(22):1929–1945